J Mater Sci (2008) 43:3976–3981
DOI 10.1007/s10853-007-2226-1

Crystallization of amorphous silicon thin films: comparison between experimental and computer simulation results

J. Kioseoglou · Ph. Komninou · G. P. Dimitrakopulos · I. P. Antoniades · M. K. Hatalis · Th. Karakostas

Received: 6 July 2007 / Accepted: 12 October 2007 / Published online: 21 March 2008

Abstract Polycrystalline silicon obtained by the crystallization of thin amorphous silicon films has been an important material for microelectronics technology during the last decades. Many properties are improved in crystallized amorphous silicon compared to the as-deposited polysilicon such as larger grain size, smoother surface, and higher-carrier mobility. In this work, the crystallization of amorphous silicon is investigated by combining transmission electron microscopy (TEM) observations and molecular dynamics calculations. TEM observations on a series of specimens have shown that the majority of the silicon grains are oriented with a ⟨110⟩ zone axis normal to the surface. In order to understand the crystallization mechanism molecular dynamic simulations were performed. It is found that the ⟨110⟩c/amorphous interface exhibits the lowest reduced interfacial energy density while the ⟨111⟩c/amorphous has the lowest reduced energy differences per unit interfacial area. The most energetically unfavorable interface is ⟨001⟩c/amorphous.

Introduction

Polycrystalline silicon in the form of thin films has been an important material for microelectronics technology during the last decades. More specifically, polysilicon thin film transistors (TFTs) have attracted great interest over the past decade or so due to their applications in the production of active matrix liquid crystal displays (AMLCDs). The relative high mobility of polysilicon TFTs relative to amorphous-phase ones results in significant advantages such as the ability to fabricate both the active matrix pixel switching elements and the peripheral driving circuitry onto a single substrate. This fact significantly lowers the production cost, and a more effective packaging of the external circuitry for projection type AMLCDs, where small size is necessary in order to lower production costs [1].

On the other hand, the fabrication of polycrystalline silicon thin-films with optimal properties is itself a challenge to which significant research effort has been devoted over the past decades. It has been shown, for example, that polysilicon thin-films obtained by solid-phase crystallization (SPC) of amorphous silicon have improved properties compared to the as-deposited polysilicon such as larger grain size, smoother surface, and higher conductivity [2]. SPC is a simple, low-cost process that results in excellent material uniformity compared to excimer laser annealing. In the SPC process, the grain size increases as the annealing temperature decreases; however, lower temperatures require longer annealing times for the crystallization process to complete. An alternative method, rapid thermal annealing (RTA), while having larger throughput, has poorer performance than SPC [3]. Combinations and variants of the two methods have also been proposed (e.g. [4–6]).

Another very important aspect of amorphous Si thin film crystallization is the orientation of the grown grains relative to the free surface. As this material is of great technological interest, several studies in the past tried to identify the microstructure that is obtained. The ⟨110⟩ texture of the grown crystals has been observed before as predominant [7]. There has been no computer simulation study ever performed to see whether this structure is indeed

J. Kioseoglou · Ph. Komninou (✉) · G. P. Dimitrakopulos · Th. Karakostas
Department of Physics, Aristotle University of Thessaloniki, 54124 Thessaloniki, Greece
e-mail: komnhnoy@auth.gr

I. P. Antoniades · M. K. Hatalis
Department of Informatics, Aristotle University of Thessaloniki, 54124 Thessaloniki, Greece

the preferred orientation when one looks at all physical processes involved. Controlling the grain orientation is a very difficult task, since nucleation is a stochastic process, requiring some kind of external template for the crystallization process [8].

Concerning numerical simulations in silicon, c-Si, silicon free surfaces, and silicon amorphous/crystalline interfaces, there have been several studies using atomistic simulations by kinetic Monte Carlo, molecular dynamics (interatomic potential methods) as well as first-principle methods. Concerning crystallization of a-Si, in particular, much previous computational work involved the study of the energy, structure and dynamical behavior of amorphous/crystalline interfaces in bulk silicon [9–11]. There have also been theoretical studies of crystal Si free surfaces focusing on the energies of various surface orientations as well as atomic reconstruction of Si bonds at the surface layer (See e.g. [12, 13]). Realistic simulation of spontaneous nucleation and crystal growth from amorphous Si by thermal annealing using molecular dynamics (constant temperature) is a challenging task under the available computer technology due to the very long simulation times required. The time consuming calculations are due to the many body character of pseudo-potentials describing atomic interactions in semi-conducting materials (see discussion in "Computational method" section). A molecular dynamics study that successfully reproduced spontaneous crystallization in a-Si under bulk conditions was presented in [14]. An interesting simulation method combining fundamental (atomic level) techniques with higher-level simulators was presented by Marques et al. [15] demonstrating recrystallization of an amorphous blob inside bulk crystalline Si in realistic time scales.

Thin film conditions impose extra difficulties, i.e., the effect of the free surface and the interactions of the Silicon layer atoms with atoms in the substrate material. The present study is a first attempt to combine an experimental and computer simulation approach in order to describe and explain crystallization of amorphous silicon thin films on a stiff substrate under low-temperature annealing. More specifically, we investigate the orientation of the obtained crystallized structures relative to the thin film free surface and, using molecular dynamics, we offer an explanation as to why the ⟨110⟩ texture is predominant in observations based on interfacial energy calculations of crystalline/amorphous interfaces of various relative orientations in thin film conditions.

Experimental

In this investigation 100-nm thick amorphous silicon films were deposited by low pressure chemical vapor deposition (LPCVD) on top of 150 mm oxidized silicon wafers. The substrate oxide thickness was 2 μm. The silicon wafers received an initial solvent clean followed by an acid clean prior to loading them into the LPCVD furnace that was held at 500 °C. The reactant gas used for the deposition of the amorphous silicon films was pure disilane and the deposition pressure was 0.16 torr. After the deposition of the amorphous silicon film, the wafers were ex-situ annealed at 600 °C in nitrogen ambient.

For the transmission electron microscopy (TEM) observations, a Jeol 2011 electron microscope, operated at 200 kV, was used with a point to point resolution of 0.19 nm and $C_s = 0.5$ mm.

TEM observations on a series of a-Si film specimens have shown that the majority of the Si grains are crystallized along a ⟨110⟩ direction. ⟨110⟩-oriented Si grains, crystallized from the amorphous phase following "dendrite" type growth, are illustrated in the two TEM micrographs of Fig. 1a and b. The corresponding ⟨110⟩ electron diffraction pattern (EDP), taken from the "dendrite" crystal of Fig. 1b, is presented in Fig. 1c. The preferred lateral growth directions are of ⟨112⟩ type, i.e., the dendrites are grown along the {111} planes and the 70.6° angle is identified between the dendrite branches. The growth mode of the ⟨110⟩ dendrites is presented in Fig. 1d. In the ⟨110⟩-oriented grains numerous {111} twins are observed as it is visible in the TEM micrograph and the corresponding EDP shown in Fig. 2a and b. A faceted $(111)/(\bar{2}11)$ twin in a dendrite crystal, viewed along $[0\bar{1}1]$, is illustrated in the high-resolution transmission electron microscopy (HRTEM) micrograph of Fig. 3.

Computational method

We use the well-known bond-order Tersoff potential [16, 17], where the total potential energy is given by

$$E = \frac{1}{2}\sum_{j\neq i} V_{ij} \tag{1}$$

where V_{ij} is the bond energy between atoms i and j

$$V_{ij} = f(r_{ij})[V_R(r_{ij}) - b_{ij}V_A(r_{ij})] \tag{2}$$

and r_{ij} is the interatomic distance.

The pair like attractive $V_A(r_{ij})$ and repulsive energies $V_R(r_{ij})$ are given as Morse-like terms. In the present study the parameter values of [16] are utilized. In order to test the suitability of the Tersoff potential for our study, the excess surface energies of {110} and {111} relaxed silicon surfaces were calculated by use of the slab geometry. This yielded 49 and 79 meV/Å^2, for the {110} and {111} surfaces, respectively. The Tersoff potential calculates the {110} surface as energetically favorable compared to the {111}, in agreement

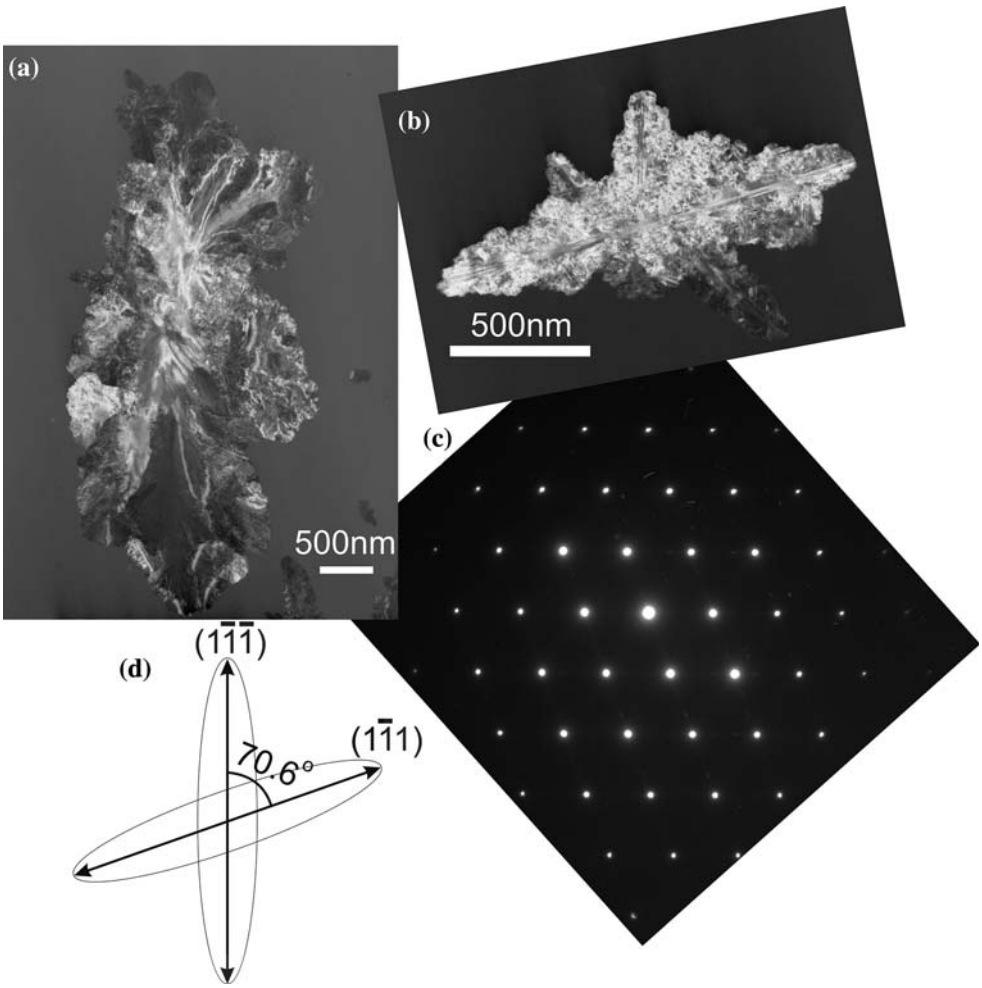

Fig. 1 (**a**) and (**b**) TEM micrographs depicting "dendrite" type Si grains crystallized along ⟨110⟩. (**c**) Electron diffraction pattern of ⟨110⟩ zone axis taken from the crystal of (**b**). (**d**) The growth mode of the ⟨110⟩ dendrites. The preferred lateral growth directions are of ⟨112⟩ type, i.e., the dendrites are grown along the {111} planes and the 70.6° angle is identified frequently between the dendrite branches

with the literature [12, 13]. It should be noted that the present calculations were carried out at 0 K.

In order to understand the crystallization mechanisms, molecular dynamics simulations were performed. As a first step, the amorphous Silicon atomic structure was obtained from crystalline Si following a well-defined procedure for amorphization [14]. In particular, a 8000-atom rectangular parallelepiped computational cell was heated from a starting temperature of 1,000 K up to 4,000 K and subsequently cooled rapidly down to the temperature of 1,700 K at a rate of 10^{14} K/s. Then, the temperature was kept constant for a 0.1 ns. Periodic boundary conditions were applied in all three directions of the computational cell. This procedure yielded an equilibrium a-Si bulk structure at 1,700 K, a temperature well below the 1,900 ± 50 K or 2,350 ± 50 K melting point of a-Si and c-Si, respectively [9].

As a second, the equilibrium a-Si structure under thin film conditions was obtained as follows: molecular dynamics simulations were performed, using the supercell of the equilibrium a-Si bulk structure obtained from the first step, by imposing free boundary conditions on one side (free surface) and fixed boundary conditions on the opposite side of the supercell, as shown in Fig. 4a. Fixed boundary conditions were applied by holding fixed at their initial positions, throughout the simulation experiments, all Si atoms within a distance of 11 Å from the boundary. These conditions effectively simulate the interactions between atoms of the interfacial area, i.e., between atoms in the silicon layer and the silicon oxide substrate. This is due to the fact that silicon atoms attached to the glass substrate are much less mobile compared to silicon atoms lying within the film and close to the free surface. Periodic boundary conditions were applied in all remaining sides. The thickness of the film (distance from free surface to fixed boundary) was 40 Å. Under the conditions described above, the computational cell was quenched to 900 K from an initial temperature of 1,700 K and by the use of the Nose-Hoover method [18, 19] it was further annealed at constant temperature for 0.5 ns. The outcome was an equilibrium a-Si thin film structure, obtained at low temperature (900 K) relative to the melting point. Since the Tersoff potential with the parameters used in the simulations overestimates the melting point of Silicon, 900 K is considered as "low" temperature.

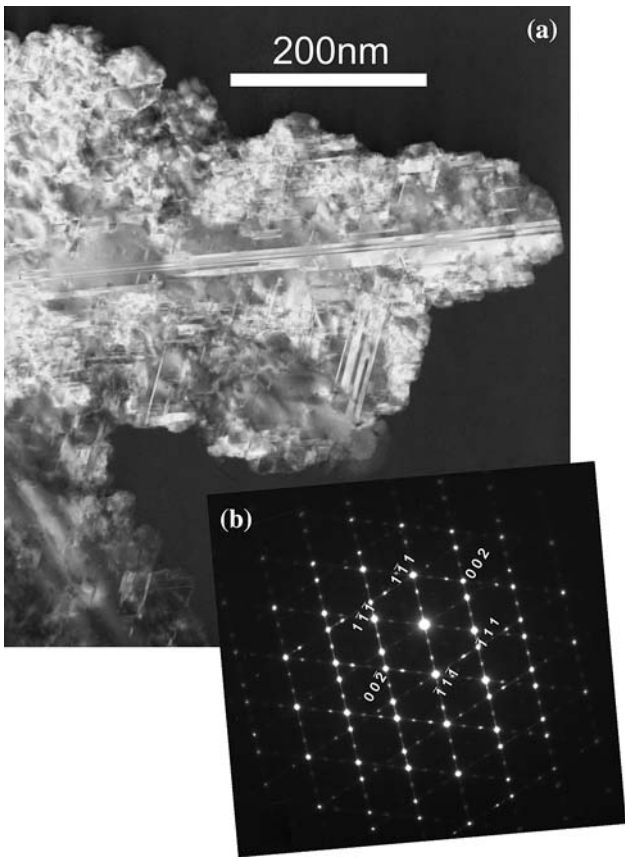

Fig. 2 (**a**) TEM micrograph showing {111} twinning in a [110]-oriented dendrite. (**b**) The corresponding electron diffraction pattern

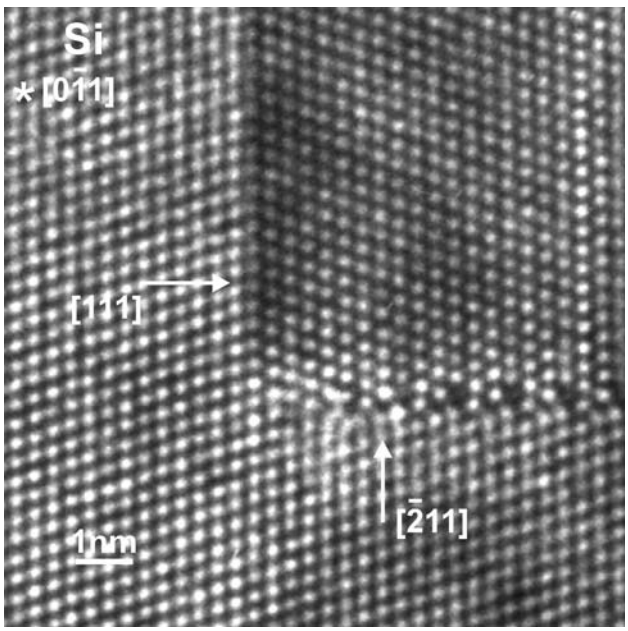

Fig. 3 HRTEM micrograph showing a faceted twin in a dendrite crystal, viewed along [0$\bar{1}$1]. The twin is facetted onto the [111] and [$\bar{2}$11] symmetry planes

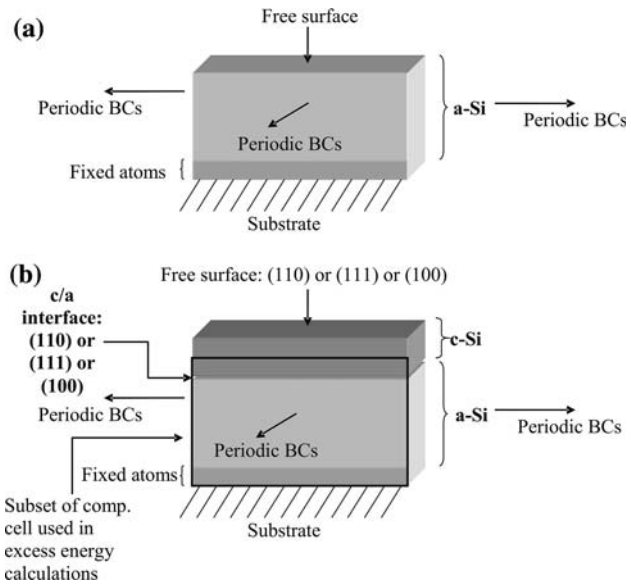

Fig. 4 (**a**) The computational cell used in the molecular dynamics simulation of an a-Si thin film. (**b**) The computational cells (one for each considered orientation of the c-Si slices) used in the molecular dynamics calculations of the c/a interface excess energies

Furthermore, crystalline parallelepiped slices (c-Si), oriented along either [001] or [110] or [111], were placed on the free surface of the equilibrium a-Si thin film structure obtained from the previous step. The thickness of the crystalline slices was of the order of 60 Å. In this way, an unrelaxed crystalline/amorphous (c/a) interface, parallel to the free surface, was created within a complex supercell which consists of the equilibrium a-Si thin film structure combined with a crystalline slice in one of the three aforementioned orientations. Free boundary conditions were applied for the simulations on the top (free) surface of the crystalline slice and fixed boundary conditions on the bottom surface of the amorphous layer, as shown in Fig. 4b. The complex supercells were annealed at a constant temperature of 900 K for 0.5 ns. In this way, the orientation-dependant stability of the crystalline/amorphous interfaces was studied. In addition, an insight as to which of the three textures is favored when crystallization of a-Si thin films occurs at low temperature annealing conditions was obtained.

The excess energy, due to each c/a interface configuration, as a function of time was calculated. Two definitions of excess energy were used: (a) the excess interfacial energy per unit area and (b) the excess interfacial energy per unit area and per interfacial atom. In order to calculate each energy, we considered a subset of the computational cell cut around each c/a interface, excluding the topmost crystal layers from the free surface, as shown in Fig. 4b, in order to subtract the free surface contribution to the energy. Then, we calculated the

difference between the total internal energy of this subset containing each of the considered c/a interfaces and the energy of a supercell of perfect Si crystal (bulk) structure containing the same number of atoms. In case (a) we divided this number by the total interface area, whereas in case (b) we divided by the total interface area and by the total number of atoms within the first layer of the crystal side of the c/a interface (interfacial atoms). Energy values were extracted as time averages of the last 0.3 ns of the simulations, when the system had reached equilibrium and average energy is thus approximately a constant. The total number of atoms of the volume used as well as the total interfacial area is the same for all three crystal orientations; however, the number of interfacial atoms differs due to the different packing density of different crystal planes in silicon. We also note that, whereas the energetic contribution of the fixed boundaries on the amorphous side is included in the excess energy calculations, it is essentially equivalent for the three orientations because the employed amorphous structure is the same in all cases. Finally, as we are only interested in a comparison of the excess energies among the three c/a orientations, our results are expressed as reduced energy differences (REDs) from the excess energy of the interface which yielded the lowest value (i.e., reduced energy difference$^{(110)} = (E^{110}_{\text{excess}} - E^{\text{favourable}}_{\text{excess}})/E^{\text{favourable}}_{\text{excess}}$). The resulting REDs for each of the three c/a orientations under consideration are shown in Table 1. The errors are estimated by the standard deviation of the energy values of the last 0.3 ns of the simulations, when the system had reached equilibrium. We notice that the c/a orientation with the lowest RED per area and per interfacial atom is $\langle 110 \rangle$, whereas the c/a orientation with the lowest RED per interfacial area is $\langle 111 \rangle$. The $\langle 001 \rangle$ texture is, by both excess energy measures, energetically unfavorable.

Table 1 Reduced interfacial energy differences per unit area and interfacial energy densities for the three interfaces

Interface	% RED per unit area (±5%)	% RED per interfacial atom and unit area (±9%)
(110)c/a	3	0
(111)c/a	0	8
(001)c/a	9	58

In Fig. 5 snapshots of the computational cells for the three c/a interfaces obtained at $t = 0.2$ ns are illustrated. Even after 0.5 ns of simulation time, no growth of the Si crystal grain occurred. This is in agreement with [14], where by iso-volume and iso-thermal molecular dynamic simulations of a-Si bulk structure at 900 K, no nucleation and subsequent crystal grain growth was observed. In that study, spontaneous nucleation and crystal growth occurred at much higher annealing temperatures and only after large simulation times.

Conclusions

The Si crystal/amorphous interfaces in Si thin films have been investigated by the use of TEM observations and for the first time in thin film conditions by constant-temperature molecular dynamics simulations based on the Tersoff interatomic potential. The TEM analysis has shown that the dominant texture of the grown crystal grains is $\langle 110 \rangle$. On the other hand, simulation results have shown that the $\langle 110 \rangle$ c/a interface exhibits the lowest RED per interfacial atom and unit interfacial area, expressing energy density, while the $\langle 111 \rangle$c/a has the lowest RED per unit area. The most energetically unfavorable interface is the $\langle 001 \rangle$c/a. Based on these results we can conclude that, for our conditions, the silicon crystallization proceeds with a way that favors the lowest interfacial energy density which results in a $\langle 110 \rangle$ dominant texture. It is known that the $\langle 110 \rangle$ direction is the close-packed direction. Therefore, it is not

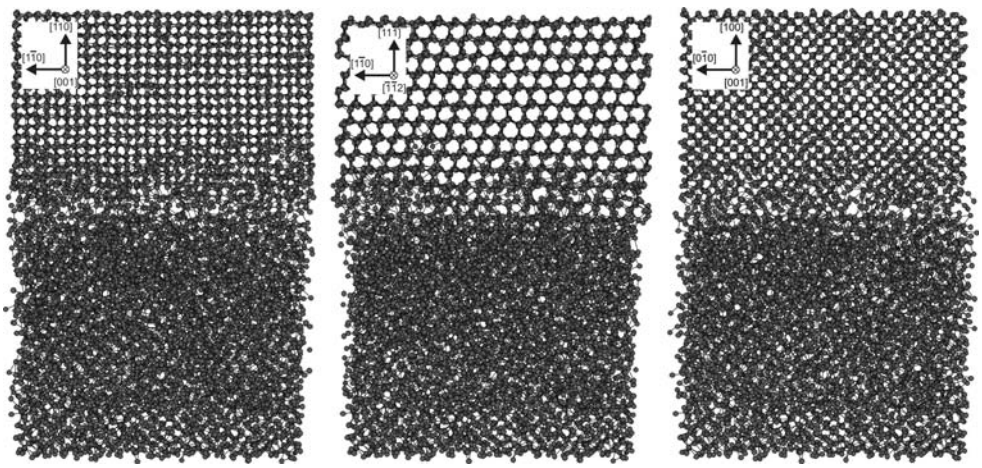

Fig. 5 Snapshots of the [110]c/a, [111]c/a and the [100]c/a interfaces annealed at 900 K for 0.2 ns

surprising that while the ⟨111⟩ zone axis is found energetically favorable with respect to ⟨110⟩ having as reference the RED per unit area, the ⟨110⟩ exhibits the lowest interfacial energy density. Regarding the experimental observations it is obvious that under our growth conditions the seed type, 3D crystallization is dominant, and consequently the Si grains are crystallized along a ⟨110⟩ direction due to the fact that the ⟨110⟩ orientation exhibits the lowest interfacial energy density.

Acknowledgements This work is co-funded by the European Social Funds and National resources through the "PYTHAGORAS II" programme.

References

1. Kouvatsos D, Voutsas AT, Hatalis MK (1999) J El Mat 28(1):19
2. Hatalis MK, Greve DW (1988) J Appl Phys 63:2260
3. Bonnel M, Duhamel N, Guendouz M, Haji L, Loisel B, Ruault P (1991) Jpn J Appl Phys 30(11B):L1924
4. Subramanian V, Dankoski P, Degertekin L, Khuri-Yakub BT, Saraswat KC (1997) IEEE El Dev Lett 18(8):378
5. Singh RK, Jung SM, Lee SM, Hummel RE (1998) J El Chem Soc 145(11):3963
6. Bo XZ, Yao N, Sturm JC (2002) J Appl Phys 91(5):2910
7. Efremov MD, Bolotov VV, Volodin VA, Fedina LI, Lipatnikov EA (1996) J Phys: Condens Matter 8:273
8. Huh H, Shin JH (2001) Appl Phys Lett 79(24):3956
9. Izumi S, Hara S, Kumagai T, Sakai S (2004) Comp Mat Sci 31:279
10. Park SH, Kim HJ, Kang KH, Lee JS, Choi YK, Kwon OM (2005) J Phys D: Appl Phys 38:1511
11. Park SH, Kim HJ, Lee DB, Lee JS, Choi YK, Kwon OM (2004) J Superlattice Microst 35:205
12. Stekolnikov AA, Furthmuller J, Bechstedt F (2002) Phys Rev B 65:115318
13. Lu G-H, Huang M, Cuma M, Liu F (2005) Surf Sci 588:61
14. Izumi S, Hara S, Kumagai T, Sakai S (2005) J Cryst Growth 274:47
15. Marques L, Pelaz L, Lopez P, Aboy M, Santos I, Barbolla J (2005) Mat Sci And Eng B 124–125:72
16. Tersoff J (1989) Phys Rev B 39:5566
17. Tersoff J (1990) Phys Rev B 41:3248
18. Hoover WG (1985) Phys Rev A 31(3):1695
19. Nose S (1990) J Phys Cond Matt 2:SA115